ADVANCED OPTICAL MATERIALS

Supporting Information

for *Adv. Optical Mater.*, DOI 10.1002/adom.202303309

2D-Material-Fused High-Emittance Plasmo–Photonic Metasurfaces

Masanobu Iwanaga, Xu Yang, Vasilios Karanikolas, Takashi Kuroda and Yoshiki Sakuma*

Supporting Information: 2D-Material-Fused High-Emittance Plasmo–Photonic Metasurfaces

Masanobu Iwanaga*, Xu Yang, Vasilios Karanikolas, Takashi Kuroda, and Yoshiki Sakuma

National Institute for Materials Science (NIMS), 1-1 Namiki, Tsukuba 305-0044, Japan

*iwanaga.masanobu@nims.go.jp

S1. REFLECTANCE SPECTRUM OF THE FUSED SYSTEM

Measured reflectance (R) spectrum of the 2D-material–metasurface fused system is plotted on the right axis in Figure S1 (black curve). The R spectrum was normalized in the range of [0, 1]. The incident light shed the system normally. The measurement setup was based on that for the micro-PL measurements described in the Experimental Section of the text. The incident light was approximately normal and the incident angle was limited to less than 0.3°. The enhanced photoluminescence (PL) spectrum is shown by a red curve, which is identical to the PL spectrum in Figure 4a. The most prominent peak at 638.9 nm corresponds to a small R dip (or emittance peak). Qualitatively, this feature agrees with the emittance spectrum shown in Figure 3b. The other PL peaks at 565 and 670 nm also correspond to the R dips (or emittance peaks) at each wavelength. Thus, particular resonances of the plasmon–photon hybrid metasurface contribute to PL intensity enhancement. We note that the R spectrum contains the optical responses of the 2D material and the metasurface; therefore, the values of R in the wavelength range below 650 nm are substantially smaller than those of the metasurface only (Figure 2b). This is because the light absorption by the 2D material reduces the value of R.

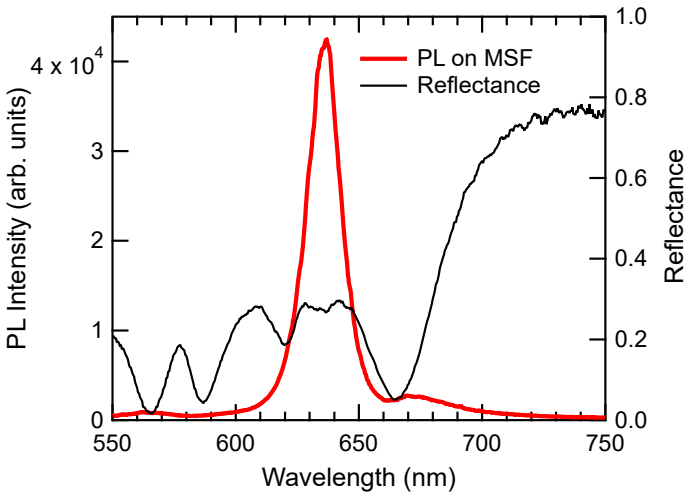

Figure S1. Comparison of the enhanced PL spectrum (red) with the normal R spectrum (black) plotted on the right axis in a normalized manner. The PL spectrum in Figure 4a is shown again for clarity.

S2. CONFOCAL IMAGE

Figure S2 shows a confocal PL image in which the analysis box for Figure 4c is indicated. The box contains 26786 pixels. The image was taken using the same sample shown in Figure 4b.

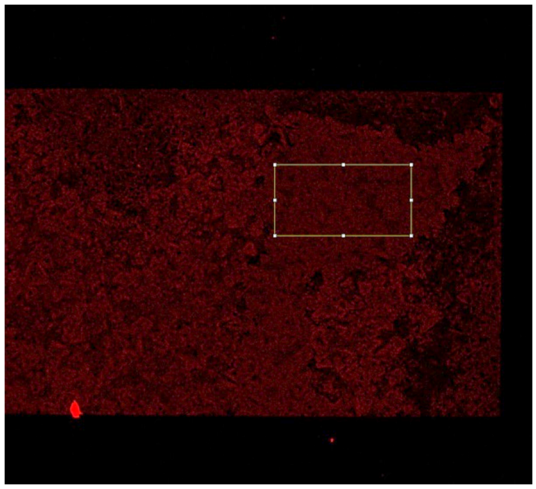

Figure S2. Confocal PL image with an analysis box (yellow).

S3. ANALYSIS FOR THE PHOTON-NUMBER DISTRIBUTION

We analyzed the photon number distribution in Figure 4c using the Poisson probability distribution, which is derived from the quantum coherent state,

$$|\alpha\rangle = \exp(-|\alpha|^2/2) \sum_{n=0}^{\infty} (\alpha^n/n!)|n\rangle,$$

and the expectation value,

$$|\langle n|\alpha\rangle|^2 = \exp(-|\alpha|^2)\,|\alpha|^{2n}/n! = \exp\,(-\langle n\rangle)\langle n\rangle^n/n!$$

where $\langle n\rangle = |\alpha|^2$, as described in a textbook [S1]. Figure S3 shows that the measured photon number distribution (red, identical to the data in Figure 4c) was reproduced fairly well by using the Poisson probability distribution. In fitting the experimental data, we used an equation such that

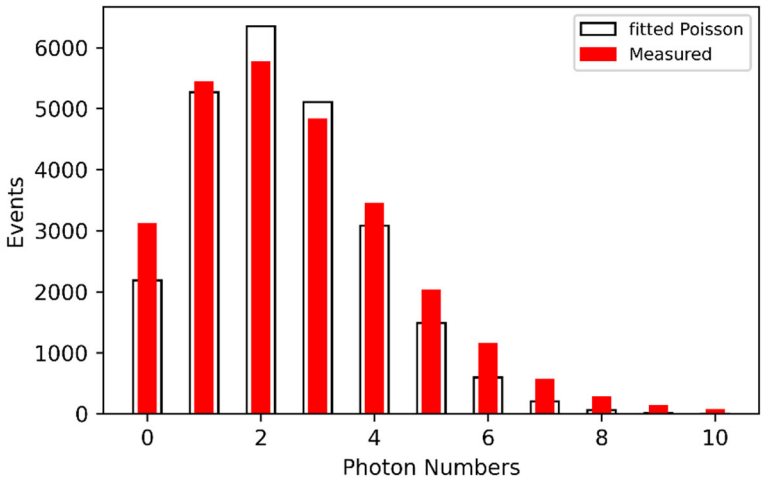

Figure S3. Measured photon number distribution (red) versus Poisson distribution (white bar).

$P(k) = a\langle n\rangle^k \exp(-\langle n\rangle)/k!$ where a is a proportional constant, $\langle n\rangle$ is the mean photon number, and k is a nonnegative integer representing the photon numbers. The fitting parameters are a and $\langle n\rangle$, which were determined to be $a = 24350$ and $\langle n\rangle = 2.41$ through the least square method. Thus, the measured distribution is reproduced fairly well. As described in the text, the Poisson distribution means that the PL is a coherent single-mode photon emission [S1] and indicates that this fused system works as a quantum light source.

S4. PURCELL FACTOR

Numerically evaluated Purcell factor is shown in Figure S4. The procedure is described in the txt (Experimental Section). The electric dipole was assumed to be 2 nm above the top of the metasurface. The direction of the dipole was set to *x*-polarized. The *x, y,* and *z* coordinates are shown in Figure 2a. It is observed that the Purcell factor takes values of 1.2–4.4 in the wavelength range of 600–700 nm.

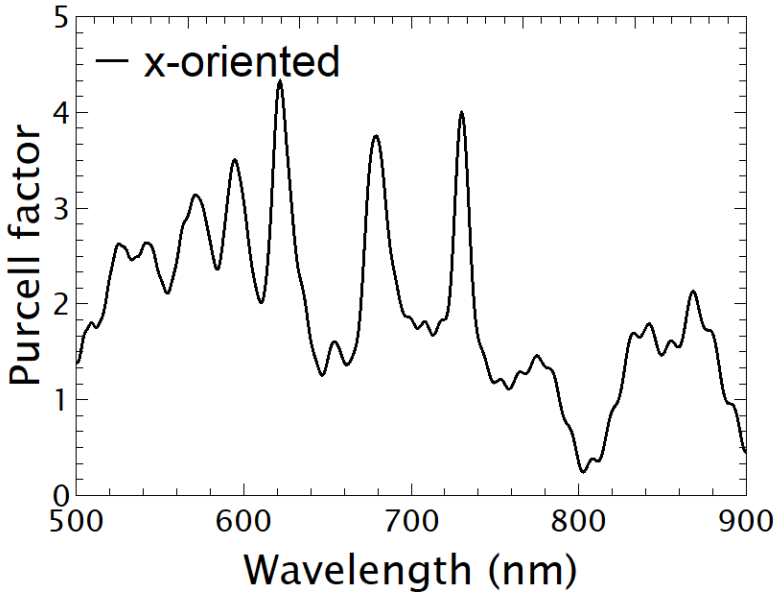

Figure S4. Purcell factor was evaluated numerically. This method is described in the text.

S5. RAMAN SCATTERING

Raman scattering spectra are compared here. Figure S5 shows the enhanced Raman scattering spectrum measured on the plasmo–photonic metasurface (purple) and an ordinary Raman scattering spectrum of the as-grown TMDC monolayer on a 2 cm square sapphire substrate (black). The former is the same as the spectrum shown in Figure 6a, displayed with an offset baseline (dashed black) in Figure S5.

The Raman peaks at 323, 351, and 418 cm^{-1} of the as-grown WS_2 monolayer are in good agreement with the Raman peaks reported in reference [43]. We observed a slight shift (~5 cm^{-1}) of the entire spectrum of the metasurface, compared to the as-grown spectrum. This probably

originated from the slight distortion of the transferred monolayer on the perforated nanostructures of the metasurface. This kind of slight shift in the Raman spectra after transfer was reported in [43].

In addition, chemical doping can change the peak positions of the Raman scattering. The as-grown Raman peaks at 378 and 398 cm^{-1}, indicated by arrows, are attributed to the Raman peaks originating from the MoS_2-like E_{2g}^1 and A_{1g} modes, respectively [48]. From the signal intensity ratio of the 351 and 378 cm^{-1} peaks, we estimated the dopant Mo to be approximately 10% [48].

Finally, we note that we measured the Raman scattering spectra at different excitation spots; as a result, the two spectra were not identical to each other, even if we neglected the wavenumber shift. However, the spectral profiles were qualitatively similar to each other.

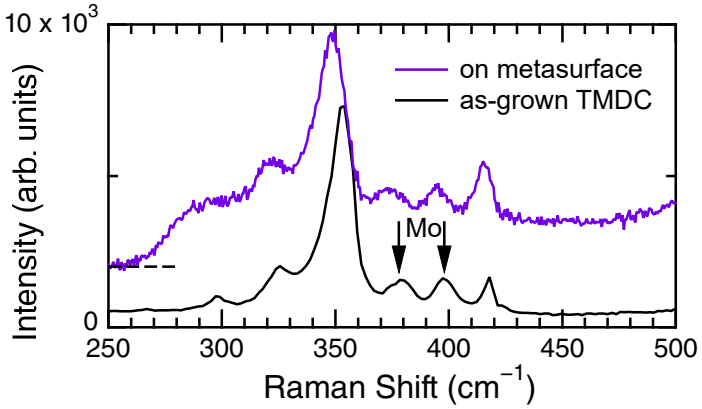

Figure S5. Enhanced Raman scattering spectrum (purple) measured on the plasmo–photonic metasurface. The as-grown Raman scattering spectrum (black) was measured on a sapphire substrate. Arrows indicate the Raman peaks originating from the dopant Mo. For clarity, the enhanced Raman spectrum is offset, and the baseline is indicated by a dashed black line.

S6. UNIFORMITY OF NANOSTRUCTURES IN THE METASURFACE

The plasmo–photonic metasurfaces were fabricated based on high-resolution electron-beam lithography, as described in the text (the Experimental Section). Here, the structural uniformity is confirmed in a wide-view scanning electron microscopy (SEM) image. Figure S6 shows the SEM image. The scale bar, consisting of 11 small white tips, is 10 μm. The circular holes are uniform in shape and size. Because the transition metal dichalcogenide (TMDC) monolayer was transferred onto the metasurface, most of the area was gray, and small portions appeared white owing to the rifts of the TMDC monolayer. The white areas correspond to the Au exposed at the outermost surface. We note that a magnified SEM image is shown in Figure 1e.

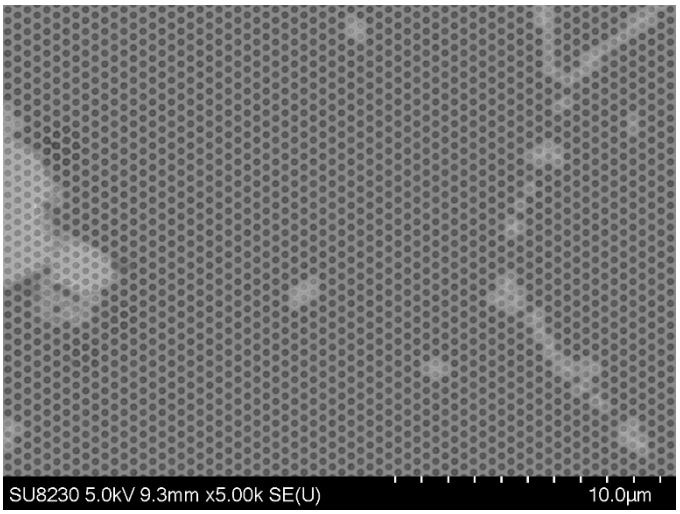

Figure S6. Wide-view SEM image of TMDC-monolayer-transferred plasmo–photonic metasurface.

Reference

[S1] R. Loudon, *The Quantum Theory of Light* 3rd ed (Oxford Univ. Press, UK, 2000) Chapter 5.